Neurobiology of Disease 156 (2021) 105407

Contents lists available at ScienceDirect

Neurobiology of Disease

journal homepage: www.elsevier.com/locate/ynbdi

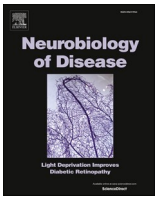

Neuritin improves the neurological functional recovery after experimental intracerebral hemorrhage in mice

Junmei Lu *, Zhaoyang Li, Qianru Zhao, Dongdong Liu, Yan-ai Mei *

Institutes of Brain Science, State Key Laboratory of Medical Neurobiology and School of Life Sciences, Fudan University, Shanghai 200438, China

ARTICLE INFO

Keywords:
Neuritin
Intracerebral hemorrhage
PERK/ATF4
Akt/mTOR
sEPSCs

ABSTRACT

Stroke is one of the leading causes of death worldwide, with intracerebral hemorrhage (ICH) being the most lethal subtype. Neuritin (Nrn) is a neurotropic factor that has been reported to have neuroprotective effects in acute brain and spinal cord injury. However, whether Nrn has a protective role in ICH has not been investigated. In this study, ICH was induced in C57BL/6 J mice by injection of collagenase VII, while the overexpression of Nrn in the striatum was induced by an adeno-associated virus serotype 9 (AAV9) vector. We found that compared with GFP-ICH mice, Nrn-ICH mice showed improved performance in the corner, cylinder and forelimb tests after ICH, and showed less weight loss and more rapid weight recovery. Overexpression of Nrn reduced brain lesions, edema, neuronal death and white matter and synaptic integrity dysfunction caused by ICH. Western blot results showed that phosphorylated PERK and ATF4 were significantly inhibited, while phosphorylation of Akt/mammalian target of rapamycin was increased in the Nrn-ICH group, compared with the GFP-ICH group. Whole cell recording from motor neurons indicated that overexpression of Nrn reversed the decrease of spontaneous excitatory postsynaptic currents (sEPSCs) and action potential frequencies induced by ICH. These data show that Nrn improves neurological deficits in mice with ICH by reducing brain lesions and edema, inhibiting neuronal death, and possibly by increasing neuronal connections.

1. Introduction

Intracerebral hemorrhage (ICH) results from vascular rupture in the brain, and is common in traumatic brain injury, brain tumors, hypertension and arteriovenous malformations, among others(Alim et al., 2019; Dai et al., 2019). ICH has high morbidity and mortality that result from both primary and secondary injury mechanisms(Dai et al., 2019), the latter of which is associated with neuronal death, inflammation, blood-brain barrier disruption, hemoglobin and disorders of blood circulation and metabolism around the hematoma(Chen et al., 2014; Lule et al., 2020; Xu et al., 2020). Since targeted treatment for the primary injury associated with ICH is limited(Chaudhary et al., 2019), a reduction in secondary injury is of therapeutic interest (Li et al., 2018). Evidence suggests that individuals with ICH suffer varying degrees of neurological dysfunction as a result of neuronal death (Li et al., 2016; Zhao et al., 2018a; Zhao et al., 2015b), and thus, maintenance of neuronal survival may be crucial to prevent ICH brain injury. Recent studies have also shown that ICH-induced secondary brain injury and neurobehavioral deficits are related to axonal damage and postsynaptic density protein (Barratt et al., 2014; Katsuki and Hijioka, 2017; Liu et al., 2018; Murphy and Corbett, 2009; Wang, 2018); therefore, the authors believe it is worth exploring if it is possible to reduce secondary damage and resulting deficits by improving synaptic transduction and neuronal excitability.

Neuritin (Nrn) is a neurotrophic factor activated by neural activity and neurotrophins (Naeve et al., 1997b; Nedivi et al., 1993). Nrn plays multiple roles during neural development by autonomously functioning in neurons to regulate the growth of dendritic and axonal arbors and to promote synaptic maturation (Naeve et al., 1997b; Son et al., 2012; Zhao et al., 2018b; Zhao et al., 2015a). In addition to its previously identified roles in neural development including synaptic plasticity, maturation and neurite outgrowth, Nrn's neurorestorative effects were observed in ischemia and traumatic brain injury (He et al., 2013; Rickhag et al., 2007), hypoxia (Le Jan et al., 2006) and in acute spinal cord injury (Gao et al., 2016). In particular, a recent study indicated that Nrn was able to attenuate early brain injury in rats after experimental subarachnoid hemorrhage by reducing brain edema and neuronal apoptosis (Zhang et al., 2017).

* Corresponding authors.
E-mail addresses: junmeilu13@fudan.edu.cn (J. Lu), yamei@fudan.edu.cn (Y.-a. Mei).

https://doi.org/10.1016/j.nbd.2021.105407
Received 12 March 2020; Received in revised form 6 May 2021; Accepted 26 May 2021
Available online 28 May 2021

Previously, we showed that Nrn stimulated the expression of potassium (K+) and T-type and L-type calcium channel α-subunits *via* insulin receptor (IR) activation in rat cerebellar granule neurons (CGNs) and cortical neurons. Importantly, we determined that the Akt/mammalian target of rapamycin signaling pathways were involved (Lu et al., 2017; Yao et al., 2012; Yao et al., 2016; Zhao et al., 2018b). We also showed that Nrn enhanced synaptic transmission in the medial prefrontal cortex and neurite length and spine density in CGNs and rat hippocampal neurons (Lu et al., 2017; Zhao et al., 2018b). Here, we determined if Nrn had a protective effect against brain injury in a collagenase VII injection mouse ICH model.

2. Materials and methods

All experiments were performed in accordance with the National Institutes of Health Guidelines for the Care and Use of Laboratory Animals. The experimental protocol was approved by the Committee on the Ethics of Animal Experiments of Fudan University (permit number: JS-020).

2.1. Experimental animals

Male C57BL/6 J mice ($N = 321$) were purchased from Slac Laboratory Animal Company (SLC Co, Ltd., Shanghai, China) and bred and maintained at Fudan University. Mice were kept under a 12-h light/dark cycle and provided with food and water *ad libitum*. Experiments were performed on 8- to 10-week-old mice (25–30 g).

2.2. Adeno-associated virus serotype 9 (AAV9) production and stereotaxic administration of AAV9 into the striatum

AAV production and stereotaxic administration of AAV9 into the striatum were performed as previously described (Karuppagounder et al., 2016; Zhang et al., 2014). Highly purified stocks of AAV9 expressing blank plasmid vectors pAAV-IRES-hrGFP (AAV9-GFP, 1.47×10^{14} v.g/mL) and overexpression mouse Nrn plasmid vectors with the CMV promoter (AAV9-Nrn, 6.00×10^{13} v.g/mL) were generated by the triple-plasmid transfection protocol, as previously described(Zhang et al., 2014). To express GFP and mouse Nrn, AAV9 was stereotaxically injected into the striatum of mice. For each mouse, 2.00 μl of AAV9-Nrn was injected into the right striatum at a flow rate of 0.15 μl/min using an SR-8 M stereotaxic manipulator (Narishige Scientific Instrument Lab, Japan) to position the syringe (1701RN-33G; Hamilton, USA) and a 130 micro-injection pump (KD Scientific, USA) to regulate injection speed. By contrast, control mice received 2.00 μl injections of AAV9-GFP. All mice received two injections as previously described at the following stereotaxic coordinates (all positions are relative to bregma): injection 1: posterior, 0.30 mm; lateral, −2.50 mm; dorsoventral, −3.30 mm; injection 2: posterior, 1.00 mm; lateral, −1.50 mm; dorsoventral, −3.50 mm. The syringe was left in place for an additional 5 min and withdrawn at a rate of 0.10 cm/min to minimize leakage of the liquid along the injection track. All mice injected with either AAV9-Nrn or AAV9-GFP virus were subjected to collagenase-induced ICH 21 days later. To confirm that the stereotaxic injections enabled the expression of Nrn specifically in the striatum, AAV9-Nrn carrying GFP was injected into the mice. Proper postoperative care was taken until the animals recovered completely. AAV9 transfection efficiency was assessed by fluorescence imaging of GFP and western blotting 3 weeks after infection.

2.3. Collagenase-induced mouse model of ICH

Collagenase-induced ICH was performed as previously described (Karuppagounder et al., 2016; Rynkowski et al., 2008). Mice were deeply anesthetized using pentobarbital sodium (50 mg/kg) and placed on a stereotaxic frame. During the procedure, the animal's body temperature was maintained at 37 °C with a homeothermic blanket. Using a 130 micro-injection pump and a Hamilton syringe, 1 μl of collagenase (0.075 U, Sigma, USA) was infused into the right striatum at a flow rate of 0.15 μl/min. Relative to the bregma point, the stereotaxic coordinates of the injection were as follows: lateral, −0.20 cm; anteroposterior, 0.62 cm; and dorsoventral, −0.35 cm. For the control group, 1 μl of normal saline was infused. The animals were randomized into Sham or ICH groups, and the identity of mice that received AAV9-GFP or AAV9-Nrn was masked to researchers who performed the ICH. Thus, in this study, the mice were divided into four groups, namely the GFP-Sham and GFP-ICH groups and the Nrn-Sham and Nrn-ICH groups. The identities of the mice were revealed after the data were collected. Proper postoperative care was taken until the animals recovered completely.

2.4. Lateral ventricle administration of PERK and Akt signaling pathway inhibitors

Inhibitors of PERK and Akt signaling pathway were administered to the lateral ventricle 30 min before the collagenase was administered. Meanwhile, daily infusions of PI103 (1 μg/μl, Selleck, USA)(Lu et al., 2011) or GSK2656157 (200 μg/μl, Selleck, USA) (Zhao et al., 2017b) were performed with a 130 micro-injection pump through the lateral ventricle (from bregma: anteroposterior, 0.5 mm; mediolateral, 1.0 mm; depth, 2.0 mm) at a rate of 0.5 μl/min for 2 weeks.

2.5. Western blot analysis

Western blot analysis was performed as previously described (Lu et al., 2017). Ipsilateral striatum tissues were lysed in RIPA lysis buffer (Beyotime Biotechnology, China) for 30 min at 4 °C. After centrifugation at 13,800 ×*g* for 20 min at 4 °C, the supernatant was mixed with 2× sodium dodecyl sulfate loading buffer and boiled for 5 min at 95 °C. Proteins were separated by 10% sodium dodecyl sulfate-polyacrylamide gel electrophoresis and transferred to a polyvinylidene difluoride membrane (Millipore, USA), blocked with 10% non-fat milk and incubated overnight at 4 °C with either anti-Nrn (1:200, Santa Cruz Biotechnology, USA), anti-p-PERK (1:500, Cell Signaling Technology, USA), anti-PERK (1:1000, Cell Signaling Technology), anti-ATF4 (1:1000, Santa Cruz Biotechnology), anti-p-Akt (1:1000, Cell Signaling Technology), anti-Akt (1:1000, Cell Signaling Technology), anti-p-mTOR (1:1000, Cell Signaling Technology), anti-mTOR (1:1000, Cell Signaling Technology), anti-GAPDH (1:1000, Beyotime Biotechnology) or anti-β-tubulin (1:1000, Beyotime Biotechnology). After extensive washing in Tris-buffered saline with 0.3% Tween 20, the membrane was incubated with horseradish peroxidase-conjugated anti-mouse or anti-rabbit IgG (1:2000, Beyotime Biotechnology) for 1 h at room temperature. Protein bands were visualized by chemiluminescence using the SuperSignal West Pico trial kit (Bio-Rad, USA) and detected using a ChemiDoc XRS system (Bio-Rad). Quantity One v.4.6.2 software (Bio-Rad) was used for background subtraction and quantification of immunoblotting data.

2.6. Behavior analysis

Open field, cylinder, corner and forelimb placement tests were used to assess sensorimotor functions (Karuppagounder et al., 2016; Rynkowski et al., 2008; Zhao et al., 2015a).

Open-field test. Locomotor activity was evaluated in each group. The open field apparatus consisted of a clear Plexiglas box (23 × 23 × 35 cm) with a black floor. Activity was detected by a computer-operated tracking system (Mobiledatum Information Technology Co., Shanghai, China) and recorded continuously over 5 min. The total horizontal distance moved was measured by the tracking system software (Mobiledatum Information Technology Co.).

Cylinder test. For the forelimb use asymmetry test, forelimb use during exploratory activity was analyzed in a transparent cylinder (10 cm in diameter and 15 cm in height). The following criteria were used

for scoring: independent use of the right or left forelimb and simultaneous use of both the left and right forelimbs to contact the wall during a full rear to initiate a weight-shifting movement. Behavioral scores were recorded by determining the number of times the right (unimpaired) forelimb (R), left (impaired) forelimb (L) and both forelimbs were used as a percentage of 20 limb usages. A single, overall limb-use asymmetry score was calculated as follows: forelimb use asymmetry score = (R − L)/20 × 100%.

Corner test. The corner task assessed the integrated sensorimotor function in both stimulation of vibrissae (sensory neglect) and rearing (motor response) (Schallert et al., 2000). Mice were allowed to proceed into a corner with a 30° angle. The direction (left or right) in which the mouse turned around was recorded for each trial. Twenty trials were performed for each mouse. The corner turn score = right/20 × 100%.

Forelimb placement test. Animals were gently held by their torsos and each forelimb was independently tested by brushing the respective vibrissae on the corner edge of a countertop. Each mouse was tested ten times for each forelimb, and the percentage of trials in which the mouse placed the appropriate forelimb on the edge of the countertop in response to vibrissae stimulation was recorded.

2.7. Measurement of the hemorrhage volume

Mice were transcardially perfused with 50 mL ice cold 0.9% (wt/vol) NaCl, and the fresh brains were coronally sectioned, each 1 mm thick. The red/pink-hued hemorrhage area in lesion side was calculated using Image J. The total hemorrhage volume was calculated by summing the hemorrhagic area of each section and multiplying by the thickness of each section(Cao et al., 2018; Shen et al., 2021).

2.8. Quantification of intracerebral hemorrhages

Cerebral hemorrhages were assessed by the spectrophotometric hemoglobin assay with Drabkin's reagent (Sigma, USA), as previously described(Xu et al., 2020). Briefly, fresh brain sections were homogenized in 500 μL distilled water, followed by sonication on ice to lyse erythrocytes and other cells. Samples were centrifuged at 15,000 *g* for 30 min at 4 °C. Supernatants were transferred to a new tube containing Drabkin's reagent, mixed and incubated at room temperature for 20 min. Optical density values were measured by spectrophotometry at 540 nm. The standard curve was generated by adding 0, 0.5, 1, 2, 4, 8, and 16 μL blood to 500 μL lysates prepared from sham brains. The calculation for hemorrhage volumes based on the standard curve by linear regression analyses(Pu et al., 2019; Yang, 2020).

2.9. Prussian Blue staining

Brain sections iron staining were executed by the Prussian blue staining with iron stain kit (Sigma, USA)(Xu et al., 2020). The Prussian blue staining was performed as followed description: brain sections were washed three times with 0.3% PBST solution for 5 min each time. After three times washing with 0.3% PBST solution, the brain sections were incubated in an iron staining working solution (1:1, 5% potassium ferrocyanide and 5% HCl) for 45 min. The slices washed in distilled water, counterstained with safranin, then covered the slides with cover slips for imaging(Dai et al., 2019; Xu et al., 2020).

2.10. Hematoxylin and eosin (H&E) staining

Brains were sectioned 3 days after induction of ICH, and H&E staining was subsequently performed on the sections as previously described (Rynkowski et al., 2008). After deeply anesthetizing the mice, brains were perfused with normal saline and 4% paraformaldehyde, rapidly harvested, fixed in 4% paraformaldehyde overnight and then incubated with 20% and 30% sucrose for 2–3 days at 4 °C. Coronal sections (20 μm) were cut using a cryostat slicer (CM1950; Leica) and stained using H&E staining buffer (Beyotime Biotechnology). Striatal lesion volume was determined by digitizing serial coronal sections (500 μm apart). A blinded observer outlined the region of brain lesions (defined by the presence of blood and/or inflammatory cells). Striatal lesion volume was determined by digitizing serial coronal sections (500 mm apart) to span the entire brain lesions.

2.11. Brain water content

Since cerebral edema formation is associated with secondary injury and outcome after ICH, we measured brain water content, as previously described (Rynkowski et al., 2008; Yang et al., 2015). Brain water content was measured 3 and 14 days after injury. For brain water content estimates, brains were immediately harvested after anesthetization. The right and left hemispheres were then dissected out, beginning 2 mm from the frontal pole. The cortex of each hemisphere was then carefully dissected from the basal ganglia. The cerebellum was retained as a control. Each of the five sections was then weighed to determine the wet weight. Brains were dehydrated over 24 h at 100 °C to obtain the dry weight. Brain water content was calculated as follows: ((wet weight − dry weight)/wet weight) × 100%.

2.12. Fluoro-Jade B (FJB) staining

Brains were coronally sectioned (20 μm) 3 days after induction of ICH, and FJB staining was subsequently performed as previously described (Cai et al., 2015; Karuppagounder et al., 2016). First, coronal brain sections (20 μm) were dehydrated sequentially in 50%, 70%, and 100% ethanol for 1, 1, and 3 min, respectively, rehydrated sequentially in 70% and 50% ethanol and phosphate buffered saline (PBS) for 1 min each, incubated in potassium permanganate (0.06%, diluted in water) for 15 min at room temperature and finally rinsed three times for 1 min each in water. After, the sections were incubated in FJB solution (0.01‰ dilute in water with 0.1% acetic acid; Merck Millipore Corporation) for 30 min at room temperature, followed by three 1-min rinses in water. Finally, the sections were dried overnight in the dark, cleared in xylene for 7 min, cover slipped with neutral balsam mounting medium (Sangon Biotech Co., Ltd., China) and dried for 24–48 h before microscopic analysis.

2.13. Luxol Fast Blue (LFB) staining

Coronal sections (20 μm) were deparaffinized, rehydrated and placed into an LFB staining solution for 2–4 h at 60 °C. The sections were then cooled to ambient temperature and excessive staining was removed by distilled water rinses for 1 min. The sections were then dehydrated in graded alcohols, cleared in xylene, cover slipped and viewed under the Olympus IX-73 microscope (Olympus, USA) to obtain images. Under the uniform shooting condition, the optical density of the LFB-stained areas was counted using ImageJ software.

2.14. Immunofluorescence

Coronal sections (20 μm) were transferred into 0.5 ml blocking solution (5% bovine serum albumin; 0.5% Triton X-100, and 0.05% sodium azide in PBS) in a multi-well plate, placed on a shaker and shaken gently for 1–2 h at room temperature. The blocking solution was then replaced with the following antibody solutions for 2 days at 4 °C: rabbit anti-GFAP (1:100, Abcam, UK), mouse anti-NeuN (1:100, Abcam) and rabbit anti-synapsin 1 (1:100, Cell Signaling Technology) in 1% bovine serum albumin, 0.5% Triton X-100, and 0.05% sodium azide in PBS. After 2 days, the antibody solution was removed and the sections were washed three times with PBST (0.1% Triton X-100 in PBS) for 10 min each, and then incubated with secondary antibody (1:1000, Thermo) for 2 h at room temperature. The antibody solution was replaced with PBST and the sections were washed three times for 10 min each in PBST. 4′, 6-

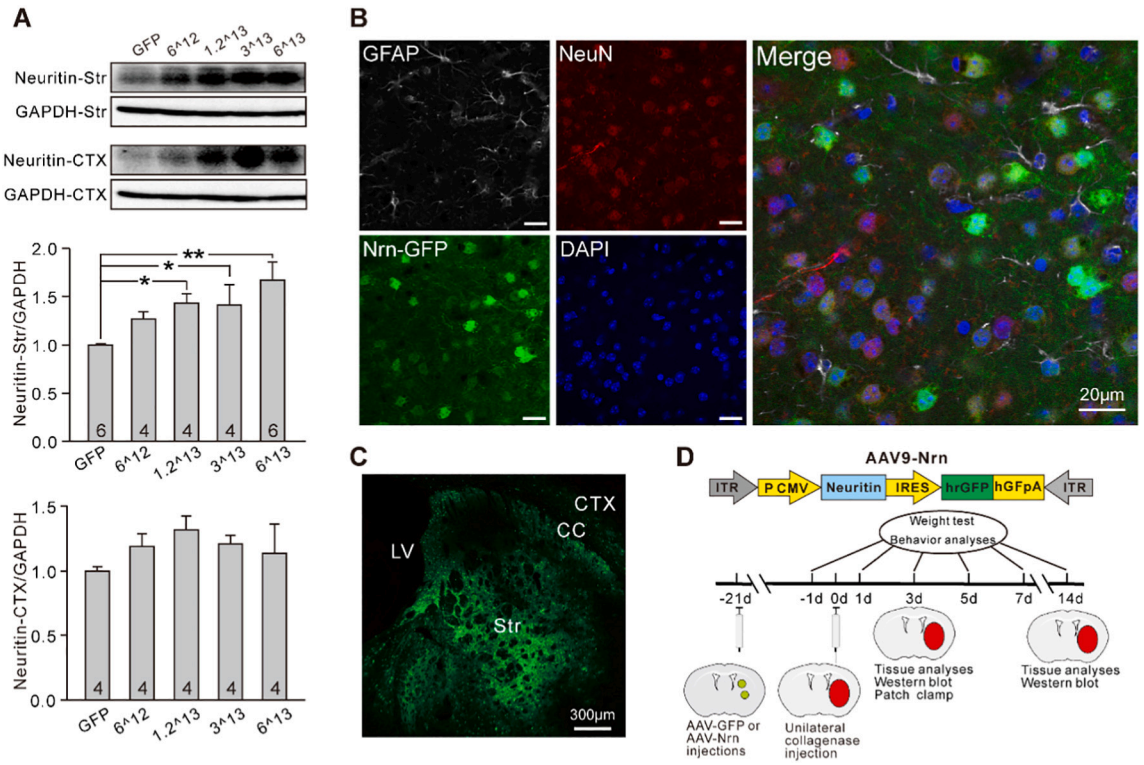

Fig. 1. Adeno-associated virus serotype 9 (AAV9) overexpressing mouse Nrn.
A, Representative western blot and bar graph showing AAV9-mediated Nrn overexpression in the striatum and cortex 3 weeks after injection (*$P < 0.05$, **$P < 0.01$ between groups connected by a straight line; one-way ANOVA). B, Immunofluorescence of GFAP (astrocytic cell marker) and NeuN (neuronal marker) in the region expressing unfused protein Nrn-GFP. C, Microscopic confocal images showing expression of the unfused Nrn-GFP protein. CTX, cortex; CC, corpus callosum; LV, lateral ventricle; Str, striatum. D, Nrn and hrGFP are coexpressed by the AAV9-Nrn vector; a diagram showing the experimental design for AAV-Nrn and the control virus that was infused into the striatum prior to ICH. Motor function and electrophysiology were measured and protein expression assayed by western blot at the indicated time.

Diamidino-2-phenylindole was then added to the slices to stain the nuclei. All sections were cover slipped using an anti-fade mounting medium, and then observed under a Zeiss LSM880 confocal laser scanning microscope (Zeiss). Immunoreactivity was examined at optimal resolution. Confocal photomicrographs were processed to adjust for scaling, brightness and contrast using LAS AF lite software (Zeiss). Under the uniform shooting condition, the optical density of synapsin 1 was counted by ImageJ software.

2.15. Acute-slice preparation

Adult mice were deeply anesthetized using pentobarbital sodium (50 mg/kg) before decapitation and rapid removal of the whole brain into an ice-cold, oxygenated (95% O_2/5% CO_2) cutting solution (220 mM sucrose, 3 mM KCl, 5 mM $MgCl_2$, 1 mM $CaCl_2$, 1.25 mM NaH_2PO_4, 26 mM $NaHCO_3$, 10 mM glucose [pH 7.3], 310–320 mOsm/l). Coronal slices containing the affected brain area were cut at 350 μm using a vibrating microtome (Dosaka, Kyoto, Japan) and incubated in oxygenated (95% O_2/5% CO_2) artificial cerebral spinal fluid (ACSF; 125 mM NaCl, 2.5 mM KCl, 2.5 mM $CaCl_2$, 1.5 mM $MgSO_4$, 1 mM NaH_2PO_4, 26.2 mM $NaHCO_3$, 11 mM glucose [pH 7.3], 300–310 mOsm/l) for 1 h at 34 °C and then stored at room temperature (Lu et al., 2017).

2.16. Patch-clamp recordings

Electrophysiology was performed as previously described (Lu et al., 2017). Recordings of slices were carried out at room temperature. Neurons selected for electrophysiological recording exhibited typical characteristics of pyramidal neurons located in layers II/III of the motor cortex. Slices were kept fully submerged during recording and continuously perfused (3–4 ml/min) with 95% O_2/5% CO_2-equilibrated ACSF. Recording electrodes were pulled from borosilicate glass on a P-97 four-stage puller (Sutter Instruments, USA), which had a resistance of 3–6 MΩ when filled with internal solution. All recordings were made using a conventional patch-clamp technique with a multiclamp 700B amplifier (Axon Instruments, USA). Data acquisition and analysis were carried out using pClamp 10.2 (Axon Instruments) and/or Origin 8 (Microcal Software, USA) software.

sEPSCs were recorded using voltage-clamp mode in ACSF with 1 μM bicuculline (Selleck,). Recording pipettes were filled with an internal solution containing 150 mM K-gluconate, 0.4 mM ethylene glycol tetraacetic acid, 10 mM 4-(2-hydroxyethyl)-1-piperazineethanesulfonic acid, 2 mM Mg-ATP, 0.1 mM Na_2-GTP and 8 mM NaCl, (pH 7.3, 290 mOsm/l). sEPSCs were analyzed using Mini-Analysis software (Synaptosoft, USA). Resting potential and action potential were recorded using the current-clamp mode in ACSF, and recording pipettes were filled with an internal solution similar to that of the sEPSCs recordings. Different intensity injection currents were used to induce action potential.

2.17. Data analysis

One- way analysis of variance (ANOVA) followed by Fisher's least significant difference post-hoc tests were used for multiple comparisons of western blot, brain water content and electrophysiology data. Two-way ANOVA followed by a post-hoc Bonferroni's test were used for behavioral analysis and weight estimate. Two-sample comparisons were performed using the unpaired Student's *t*-tests. Data are presented as the mean ± standard error. A value of $p < 0.05$ was considered statistically significant. All experiments were performed in a blinded manner.

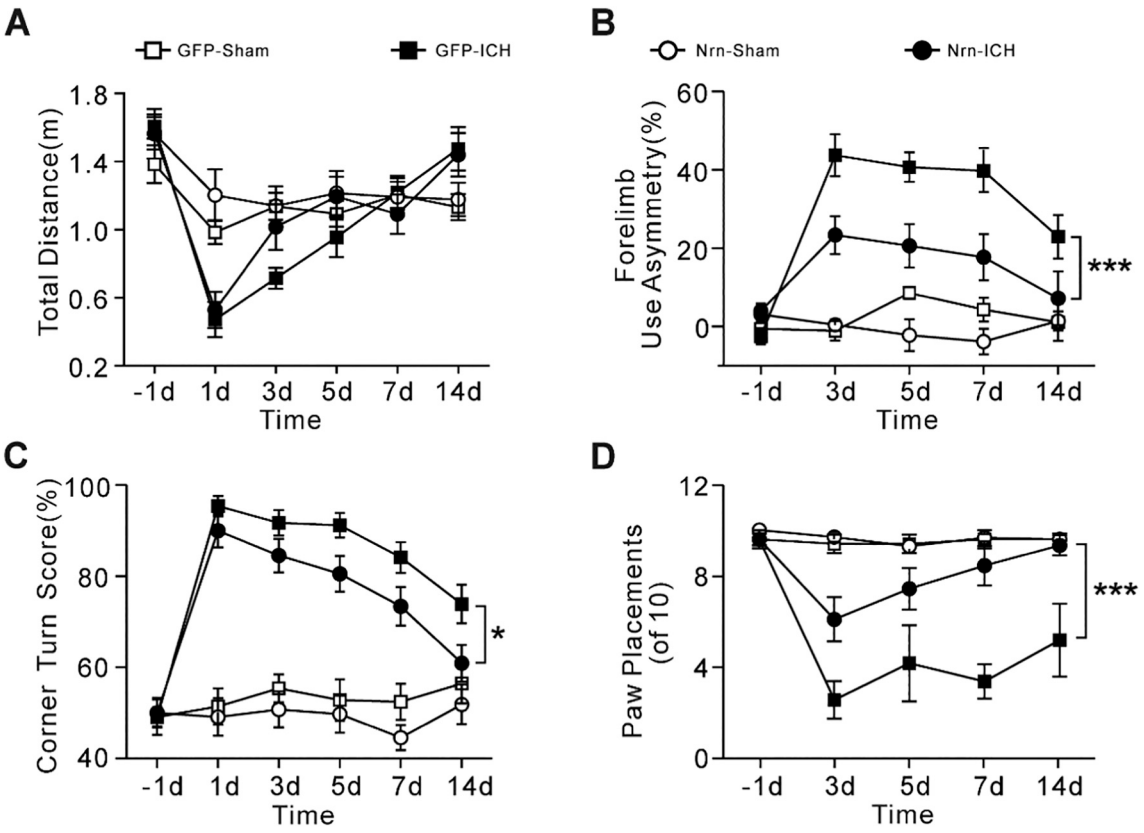

Fig. 2. AAV9 overexpressing mouse Nrn significantly improved sensory-motor dysfunction caused by intracerebral hemorrhage (ICH).
A, The effect of Nrn on the locomotor activity of mice was evaluated using the total distance travelled in the open field test (GFP-Sham, $N = 9$; GFP-ICH, N = 9; Nrn-Sham, N = 9; Nrn-ICH, $N = 10$). B, Asymmetric left forelimb results in the cylinder test (GFP-Sham, $N = 14$; GFP-ICH, $N = 15$; Nrn-Sham, $N = 13$; Nrn-ICH, N = 13). C, Corner turn score in the corner test (GFP-Sham, $N = 25$; GFP-ICH, N = 25; Nrn-Sham, $N = 22$; Nrn-ICH, $N = 25$). D, Paw placements in the forelimb placement test (GFP-Sham, $N = 5$; GFP-ICH, N = 5; Nrn-Sham, N = 10; Nrn-ICH, N = 9; $^{*}P < 0.05$, $^{***}P < 0.001$ between the GFP-ICH and Nrn-ICH groups; two-way ANOVA).

3. Results

3.1. Nrn significantly improved neurological dysfunction caused by ICH

First, we used AAV9 overexpressing mouse Nrn protein and validated its infection efficiency. All mice were injected with either AAV9-Nrn or AAV9-GFP 3 weeks prior to inducing ICH with collagenase. To determine the expression efficiency of Nrn induced by the AAV9-Nrn expression system and to obtain the effective titers for use in the next study, different titers of the AAV9-Nrn virus diluted with 0.01 M phosphate buffer saline (PBS) were used. The protein levels in striatal and cortical areas were then assessed using western blotting. As shown in Fig. 1A, the expression level of Nrn in the striatum was titer dependent and the concentration associated with the highest expression level of Nrn was 6.00×10^{13} v.g/ml, which was 67.03% higher than that of the GFP group. Meanwhile, the expression level of Nrn in the cortex of the corresponding area also increased with increasing titer. For subsequent experiments, we conducted the study using a virus with a titer of 6.00×10^{13} v.g/ml. To confirm whether the stereotaxic injections of AAV9-Nrn enabled expression specifically in the striatum, AAV9-Nrn was injected into a mouse strain using a two-point injection method as previously described (Karuppagounder et al., 2016). The experimental results showed that on the side in which AAV9-Nrn carrying GFP was injected, Nrn was mainly expressed in neurons, although low expression was occasionally evident in astrocytes (Fig. 1B). Moreover, GFP was expressed primarily in the striatum, while low expression was also observed in the corpus callosum and cortex (Fig. 1C). Fig. 1D illustrates the plasmid combination of AAV9-Nrn and the time course of all neurological outcome measurements; baseline evaluations were conducted the day prior to ICH, and behavioral tests were performed 1–14 days after ICH.

Previous studies have indicated that ICH-induced striatal injury significantly affects the sensory and motor functions of mice. In order to observe the effect of overexpression of Nrn following striatal injury, locomotor activity was first evaluated using the open field test. The results showed that there is no significant difference in the total distance travelled between the Nrn-ICH group and GFP-ICH group (Fig. 2A). There were also no significant differences in the average speed, the central distance and the central time between the Nrn-ICH group and the GFP-ICH group (data not show). Next, we examined the effect of Nrn overexpression on sensorimotor function in ICH mice using the cylinder, corner and forelimb tests (Fig. 2B–D). Baseline evaluations were conducted the day prior to ICH, and behavioral tests were performed 1–14 days after ICH. The results of the behavioral tests showed that there were no significant differences between the GFP-Sham and Nrn-Sham groups. However, compared with the GFP-ICH group, the Nrn-ICH group showed a significant improvement in neurofunctional deficits evaluated with the cylinder, corner and forelimb tests from day 3 to day 14 after ICH. Mice in the Nrn-ICH group showed a significantly reduced proportion of single limb standing in the cylinder test and biased head movement in the corner test, compared with mice in the GFP-ICH group (Fig. 2B, C), while the number of forelimb responses in the contralateral side of the lesion was significantly increased (Fig. 2D). Considering these results and the possible neuroprotective effects of Nrn following early brain injury, all further studies were performed 3 days after ICH induction, except where explicitly stated otherwise.

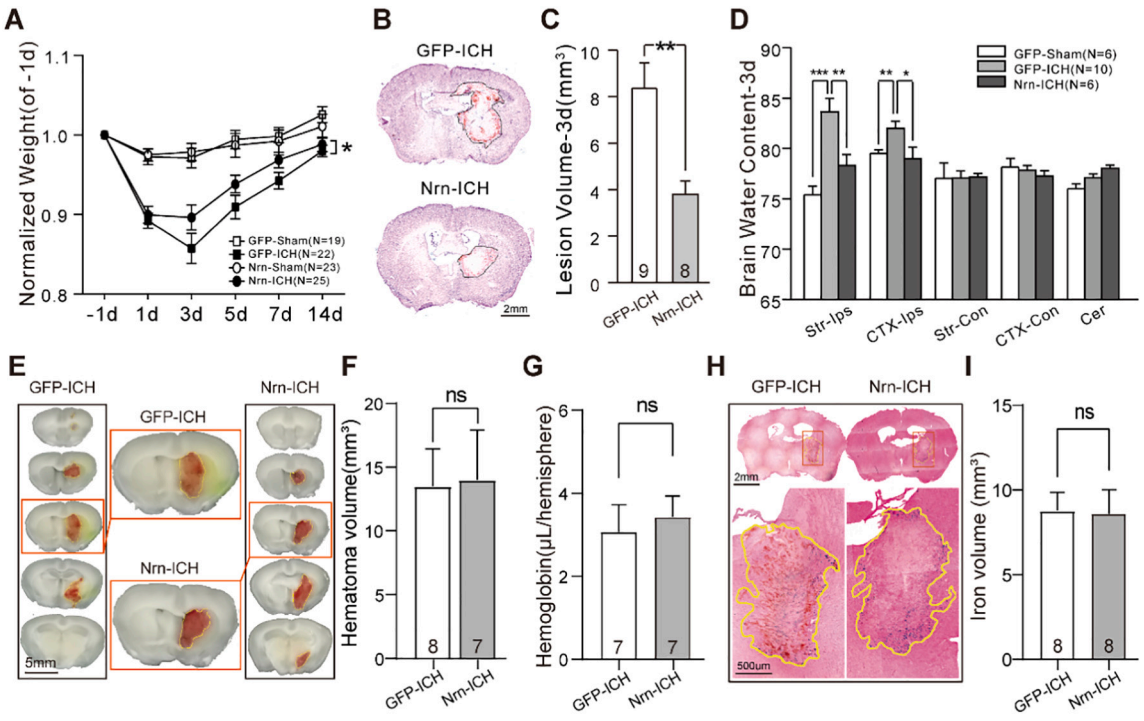

Fig. 3. Nrn reduced weight loss, brain lesions and cerebral edema induced by ICH, but didn't promote hematoma clearance.
A, The relative weight curve of each group at different time points (*$P < 0.05$ between the GFP-ICH and Nrn-ICH groups; two-way ANOVA). B, Schematic diagram of H&E staining in the GFP-ICH and Nrn-ICH groups was performed 3 days after ICH. C, Statistical histogram of brain lesion volume measured by H&E staining (**$P <$ 0.01 between groups connected by a straight line; two-sample *t*-test). D, Statistical histogram of water content in different brain areas 3 days after ICH, respectively. Str, striatum; CTX, Cortex; Cer, cerebellum; Ips: ipsilateral; Con, contralateral (*$P < 0.05$, **$P < 0.01$, ***$P < 0.001$ between groups connected by a straight line; one-way ANOVA). E, Representative serial coronal brain sections showing red-hued hematoma in GFP or Nrn mice on day 3 after ICH. F, Quantification of hematoma volumes based on photographs of consecutive brain section at 3 days after ICH. (ns $P > 0.05$ between groups connected by a straight line; two-sample t-test). G, Quantification of Hemoglobin content in the lesioned hemisphere at 3 days after ICH. (ns $P > 0.05$ between groups connected by a straight line; two-sample t-test). H, Coronal brain sections stained for iron in GFP or Nrn mice mice at 3 days after ICH. The red-boxed insets are higher-magnified views with hematoma outlined. I, Histogram shows quantification of iron$^+$ volume at 3 days after ICH. (ns $P > 0.05$ between groups connected by a straight line; two-sample t-test). (For interpretation of the references to colour in this figure legend, the reader is referred to the web version of this article.)

3.2. Nrn reduced loss weight, lesion volumes and cerebral edema induced by ICH, but didn't change hematoma clearance

Besides the improvement of behavioral function after ICH, Nrn significantly alleviated weight loss caused by ICH. Compared with the GFP-ICH group, the Nrn-ICH group showed decreased weight loss and more rapid weight gain toward baseline levels (Fig. 3A). It has been reported that the extent of brain lesions and edema is related to the progress of secondary injury after ICH; therefore, we observed the effect of overexpression of Nrn on ICH-induced brain lesions and edema. The volume of ICH-induced brain lesions was measured 3 days after ICH with H&E staining. As shown in Fig. 3B, C, the brain lesion volume in the GFP-ICH group and Nrn-ICH group was 8.36 ± 1.09 mm^3 and 3.79 ± 0.57 mm^3, respectively. Overexpression of Nrn significantly reduced ICH-induced brain lesion by 54.67%. Meanwhile, brain hemispheres ipsilateral and contralateral of the lesions were taken from mice 3 days after ICH, and the water content of striatal, cortical and cerebellar regions was measured. The results showed that, compared with the GFP-Sham group, the water content of the striatum and cortex in the ipsilateral lesion of the GFP-ICH group 3 days after ICH significantly increased from 75.38% ± 0.86% to 83.63% ± 1.32% and from 79.50% ± 0.36% to 81.99% ± 0.71%, respectively, whereas that of the Nrn-ICH group increased to only 78.28% ± 1.08% and 78.99% ± 1.12%, respectively (Fig. 3D). Considering these results, Nrn reduced loss weight, lesion volumes and cerebral edema induced by ICH.

On the other hand, we also evaluated hematoma evolution 3 days after ICH using freshly prepared thick brain sections, hemoglobin measurement and histological iron staining. First, the gross distribution of ICH was examined on freshly prepared thick brain slices (Fig. 3E, F). The hematoma volumes of Nrn-ICH group were not significantly reduced compared with GFP-ICH group. As shown in Fig. 3F, the hematoma volumes in the GFP-ICH group and Nrn-ICH group were 13.53 ± 2.91 mm^3 and 14.01 ± 3.88 mm^3, respectively. Second, blood contents in tissue homogenates of saline-perfused brains were also quantified using a spectrophotometric hemoglobin assay (Fig. 3G). Nrn-ICH group mice hemoglobin contents had no significant difference compared with GFP-ICH group mice (The hemoglobin volumes of Nrn-ICH group and GFP-ICH group were 3.07 ± 0.66 μL and 3.43 ± 0.50 μL, respectively.). Third, histological iron staining also demonstrated no significant difference ferric iron deposition between GFP-ICH group and Nrn-ICH group (The iron volume of Nrn-ICH group and GFP-ICH group were 8.76 ± 1.11 mm^3 and 8.60 ± 1.42 mm^3, respectively.) (Fig. 3H, I). Together, the results of quantification of hematoma volume, hemoglobin content, and iron deposition confirmed that overexpression of Nrn doesn't promote hematoma clearance in ICH.

3.3. Nrn reduced ICH-induced neuronal death and regulated a cell survival signaling pathway

We next detected whether overexpression of Nrn relieved ICH-induced neuronal death 3 days after ICH with FJB staining. A schematic drawing of the brain regions with FJB staining (black box) and western blotting (yellow region) is shown in Fig. 4A. The number of FJB-positive cells in the brain tissue on the ipsilateral side of the lesion in the GFP-ICH group was 164.01 ± 8.74 /mm^2, and reduced to 115.58 ± 14.53 /mm^2 in the Nrn-ICH group (Fig. 4B, C). Overall, Nrn significantly

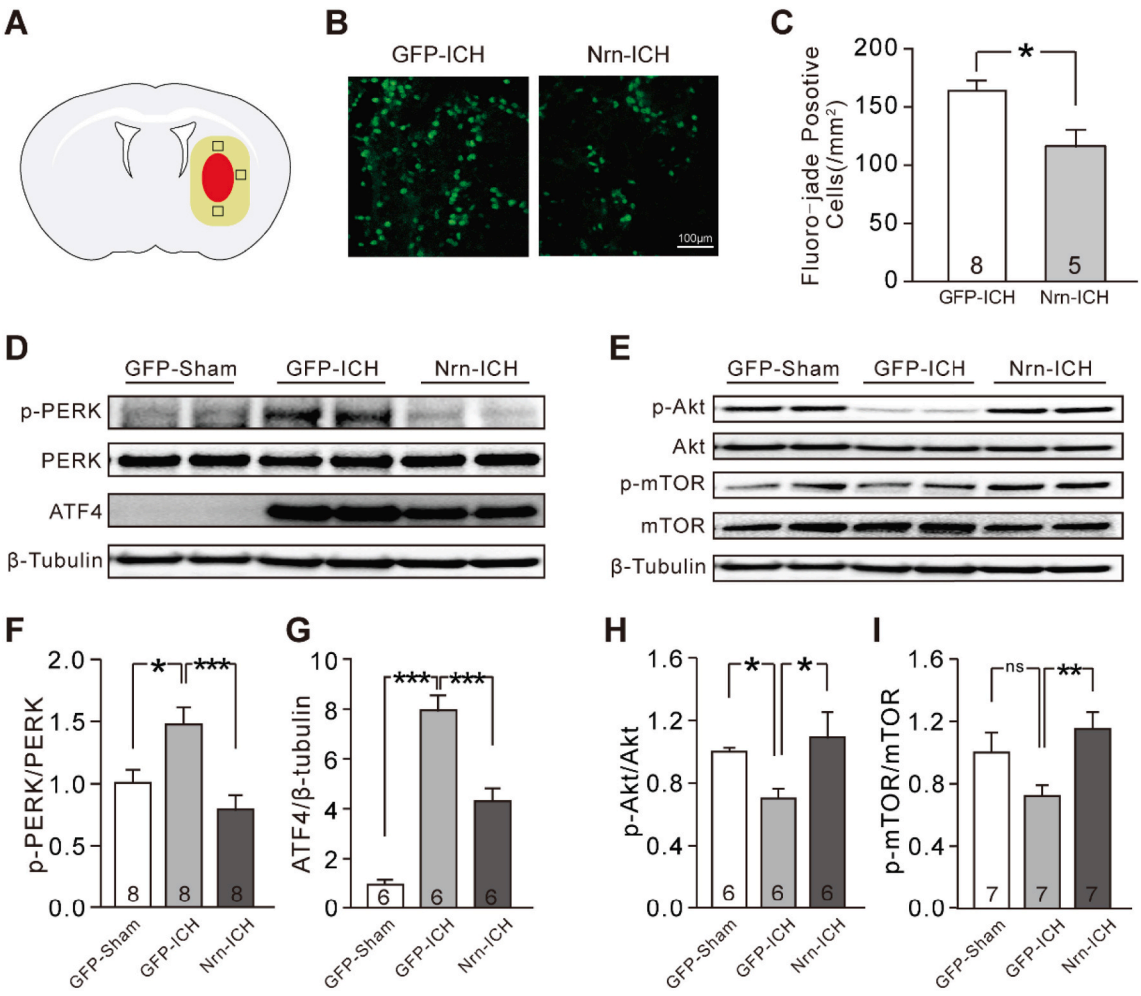

Fig. 4. Nrn reduced neuronal death and regulated the PERK/ATF4 and Akt/mTOR pathways 3 days after ICH.
A, Schematic diagram of brain regions for Fluoro-Jade staining (black box) and western blotting (yellow region). B, Nrn reduced neuronal degeneration as assessed by FJB staining (green) in the perihematomal regions of the mouse brain. C, Stereological counting of FJB–positive neurons confirmed that Nrn treatment decreased the number of injured neurons in the perihematomal regions (*$P < 0.05$ between the GFP-ICH and Nrn-ICH groups; two-sample t-test). D, Representative western blot of PERK and ATF4 expression in the ipsilateral striatum of mice in the GFP-ICH and Nrn-ICH groups. E, Representative western blot of Akt and mTOR expression in the ipsilateral striatum of mice in the GFP-ICH and Nrn-ICH groups. F-G, Statistical histogram of PERK protein phosphorylation levels and ATF4 protein expression levels. H—I, Statistical histogram of Akt and mTOR protein phosphorylation levels (ns $P > 0.05$, *$P < 0.05$, **$P < 0.01$, ***$P < 0.001$ between groups connected by a straight line; one-way ANOVA). (For interpretation of the references to colour in this figure legend, the reader is referred to the web version of this article.)

improved the cell survival rate by 29.53%.

The PERK/ATF4 pathway has been implicated in cell death induced by early brain injury after subarachnoid hemorrhage and traumatic brain injury (Rubovitch et al., 2015; Yan et al., 2017). To determine whether PERK/ATF4 signaling was involved in ICH-induced cell death and the effects of Nrn on this pathway, the levels of phosphorylated (p)-PERK and ATF4 in ipsilateral striatal tissue 3 days after ICH was detected by immunoblotting. The western blot results showed that the level of p-PERK in the GFP-ICH group was significantly higher than that in the GFP-Sham group, while p-PERK in the Nrn-ICH group decreased by 46.33% relative to the GFP-ICH group and 20.82% relative to the GFP-Sham group (Fig. 4D, F). Meanwhile, expression levels of ATF4, a known downstream protein of PERK, were significantly different between the GFP-ICH and Nrn-ICH groups. ATF4 protein expression in the GFP-ICH group significantly increased by 693.68% ± 60.97% compared with that in the GFP-Sham group, and the expression of ATF4 in the Nrn-ICH group increased by 330.45% ± 52.23% compared with that in the GFP-Sham group, which was 45.77% lower compared with that in the GFP-ICH group (Fig. 4D, G).

As previous studies have indicated that Nrn-induced activity is associated with activation of the Akt/mTOR pathways, which are commonly associated with cell survival, the effects of Nrn over-expression on these pathways were determined. Western blotting results showed that, compared with the GFP-Sham group, the p-Akt level in the ipsilateral striatum of the GFP-ICH group was significantly reduced by 30.02% ± 6.07% (Fig. 4E, H). Similarly, the p-mTOR level in the GFP-ICH group was reduced by 27.76% ± 6.58% (Fig. 4E, I). However, the p-Akt and p-mTOR expression levels in the Nrn-ICH group were at levels similar to those found in the GFP-Sham group (compared with the GFP-Sham group, the levels of p-Akt/p-mTOR in the Nrn-ICH group were increased by 9.03% ± 15.75% and 15.26% ± 11.00%, respectively.) (Fig. 4E–I).

The above results indicate that the PERK/ATF4 and Akt/mTOR pathways were involved in the protective effects of Nrn against ICH-induced neuronal death.

3.4. Nrn significantly alleviated the synaptic damage and low excitability induced by ICH

In order to study whether alterations in synaptic transmission were involved in ICH-induced dysfunction and if neuritin expression had an effect on this alteration, we first recorded sEPSCs from visually

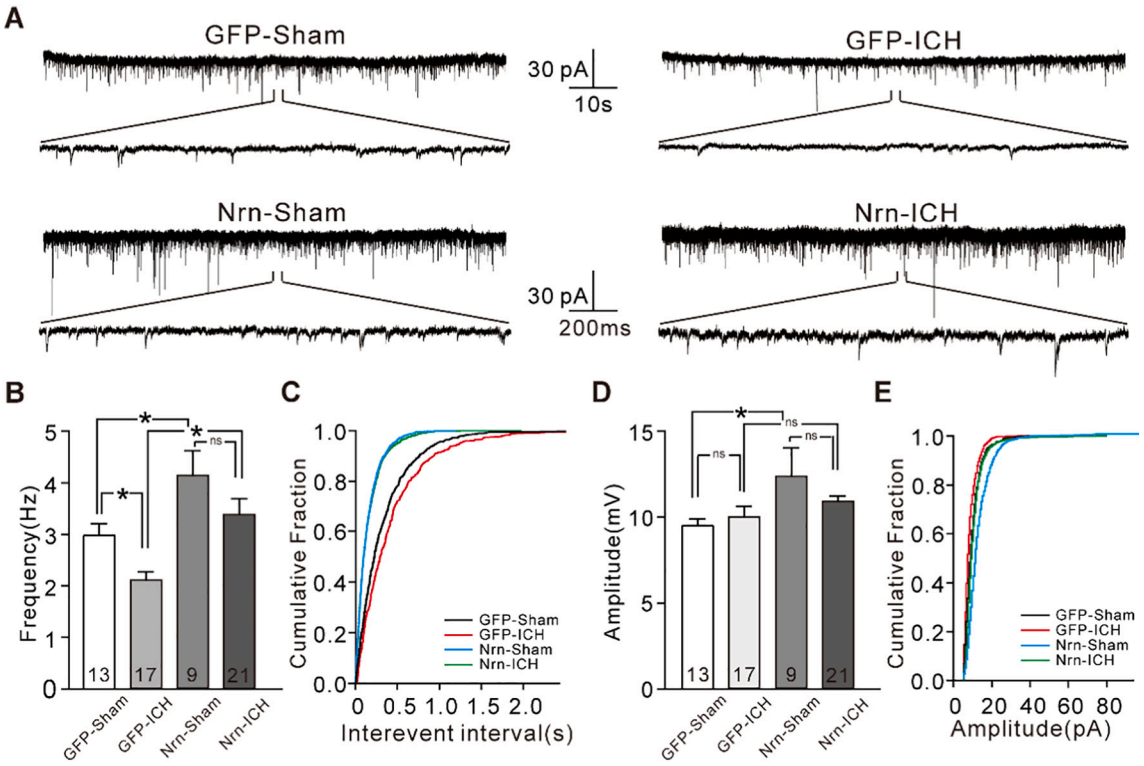

Fig. 5. Nrn rescued ICH-induced decreases in sEPSC frequency.
A, Representative sEPSC recordings from pyramidal neurons in the motor cortex. B—C, Statistical histogram and cumulative distribution plots showing the effects of AAV-mediated Nrn overexpression on sEPSC frequency. D–E, Bar graph and cumulative distribution plots showing the effect of AAV-mediated Nrn overexpression on sEPSC amplitude (ns $P > 0.05$, $^{*}P < 0.05$, between groups connected by a straight line; one-way ANOVA).

identified pyramidal neurons in the motor cortex layer II/III of brain slices, which receive signal projection from the striatum *in vivo*, using whole-cell voltage clamping. sEPSCs were recorded at a holding potential of −70 mV in the presence of 10 μM bicuculline to inhibit $GABA_A$-mediated inhibitory postsynaptic currents. Three days after ICH, the sEPSC frequency was decreased from 2.98 ± 0.22 Hz in pyramidal neurons in GFP-Sham mice to 2.12 ± 0.16 Hz in pyramidal neurons in GFP-ICH mice. Overexpression of Nrn significantly improved ICH-induced synaptic damage, and the sEPSC frequency of Nrn-ICH mice increased to 3.39 ± 0.31 Hz (Fig. 5A, B). Compared with the GFP-Sham group, the sEPSC frequency in the Nrn-Sham group increased by 39.30% (from 2.98 ± 0.22 Hz to 4.15 ± 0.47 Hz), which is consistent with results from our previous study (Lu et al., 2017). Importantly, there was no difference between the sEPSC frequency in the Nrn-Sham group and the Nrn-ICH group. Meanwhile, compared with pyramidal neurons from the GFP-Sham group, the sEPSC amplitude of pyramidal neurons from the Nrn-Sham group increased by 30.48%; however, there was no difference in the sEPSC amplitude between the GFP-Sham group and GFP-ICH group, the Nrn-Sham group and Nrn-ICH group, or the GFP-ICH group and Nrn-ICH group (Fig. 5A, D). Representative cumulative distributions of interevent intervals and amplitudes of sEPSCs are shown in Fig. 5C and E.

To test if ICH induction changed the excitability of the cortical pyramidal neurons, we used the whole-cell current-clamp technique to measure action potential (AP) and membrane potential of pyramidal neurons. Our data showed that, when neuronal APs were elicited with 100 pA injection current, AP firing frequency in pyramidal neurons of GFP-ICH mice was 22.09% lower than that in GFP-Sham mice (Fig. 6A, B). Compared with the GFP-ICH group, the AP firing frequency of pyramidal neurons in Nrn-ICH mice increased by 27.19%, whereas no significant difference was found compared with the Nrn-Sham group (Fig. 6A, B). AP amplitude and resting potential showed no significant difference among the four groups (Fig. 6C, D). Meanwhile, when neuronal APs were elicited with 100 pA injection current, we found that compared with the GFP-Sham group, the AP delay time and threshold in the GFP-ICH group were increased from 10.95 ± 1.38 ms to 17.47 ± 1.91 ms, and from −39.19 ± 0.60 mV to −37.81 ± 0.67 mV, respectively (Fig. 6E-G). In the Nrn-ICH group, the AP delay time and threshold were restored to 12.45 ± 1.22 ms and − 39.17 ± 0.71 mV compared with the GFP-ICH group, respectively (Fig. 6E–G). Taken together, these data suggest that Nrn enhanced neuronal excitability by increasing AP frequency, which might result from the decrease of the action potential delay time and threshold of pyramidal neurons in the motor cortex of mice subjected to ICH.

Accordingly, we assessed the neural network integrity of mice after ICH in terms of white matter and synaptic integrity. Then, we used LFB staining and synapsin 1 immunofluorescence staining, respectively, to observe the white matter and synaptic integrity in mice. The LFB staining results showed that the LFB optical density in the corpus callosum and striatum of mice in the GFP-ICH group decreased by 15.78% and 17.57%, respectively, compared with that of mice in the GFP-sham group. The LFB optical density in the corpus callosum and striatum of mice in the Nrn-ICH group decreased by 5.16% and 8.60%, respectively, compared with the GFP-Sham group and increased by 12.62% and 10.88% compared with the GFP-ICH group in the corpus callosum and striatum, respectively (Fig. 7A–C). We observed a similar pattern in synapsin 1 immunofluorescence staining. The synapsin 1 optical density in the cortex and striatum of mice in the GFP-ICH group was reduced by 63.99% and 34.21%, respectively, compared with that of the GFP-Sham group. Compared with mice in the GFP-Sham group, the optical density of synapsin 1 in the cortex and striatum of mice in the Nrn-ICH group was reduced by 22.56% and 7.86%, respectively. Finally, the synapsin 1 optical density in the cortex and striatum of mice in the Nrn-ICH group was increased by 115.06% and 40.04%, respectively, compared with

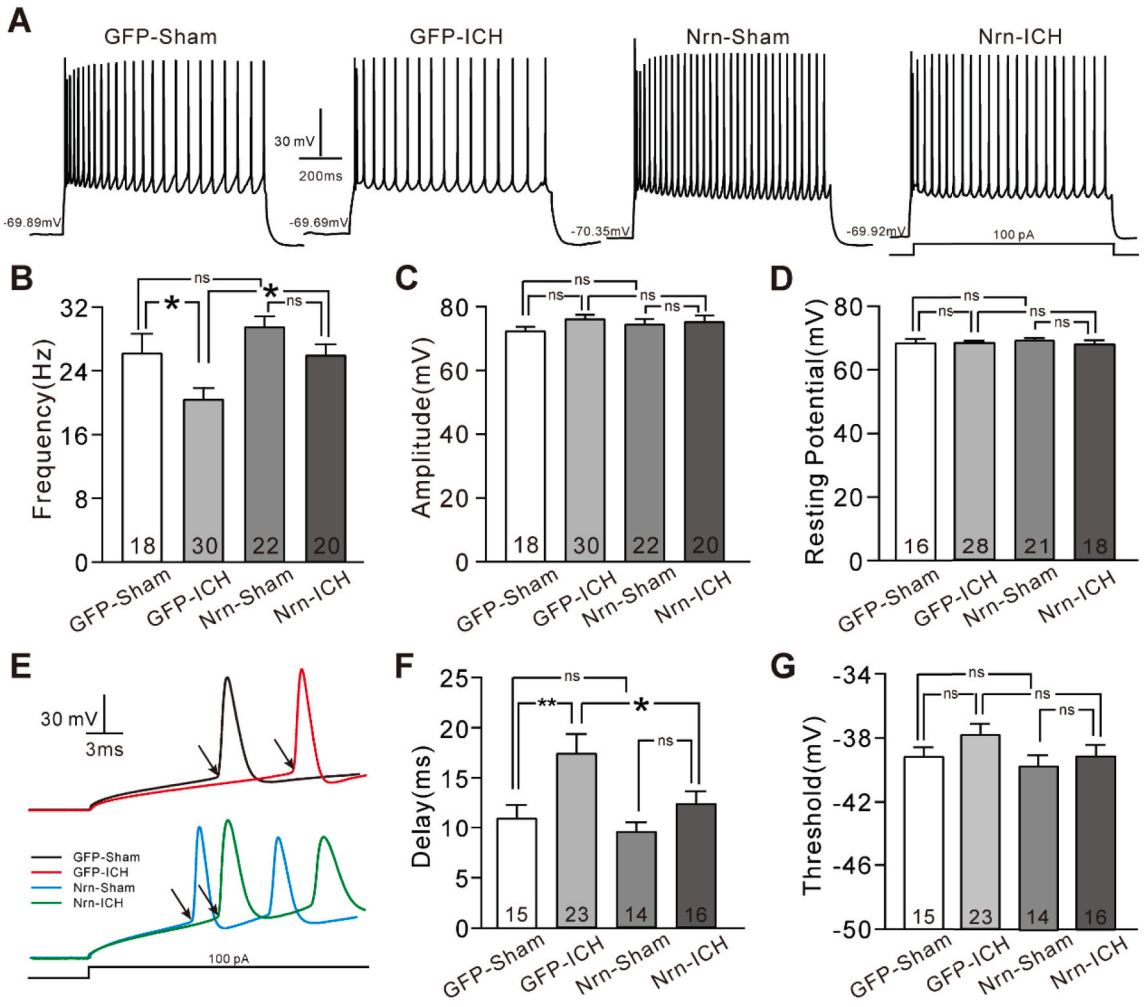

Fig. 6. Nrn significantly improved ICH-mediated low neuronal excitability in motor neurons.
A, Representative action potential (AP) recordings from the neurons in the motor cortex. B—C, Effect of AAV-mediated Nrn overexpression on AP firing frequency and amplitude when the injected current is 100 pA. D, Effect of AAV-mediated Nrn overexpression on resting potential. E, Representative action potential recordings of the first AP. F–G, The statistical histogram of delay time and threshold. (ns $P > 0.05$, $^{*}P < 0.05$, $^{**}P < 0.01$ between groups connected by a straight line; one-way ANOVA).

that of mice in the GFP-ICH group (Fig. 7D–F). Taken together, these data indicate that white matter and synapse integrity are better preserved because of Nrn-overexpression.

The above results indicate that it is high likely that Nrn improved synaptic transmission and low excitability induced by ICH *via* enhancement of white matter and synapse integrity.

3.5. *The effect of Nrn on brain lesions, edema and neuroprotection in the later stages of ICH*

The effect of Nrn on brain lesions, edema and neuroprotection in the later stages of ICH was observed. The volume of ICH-induced brain lesions was measured 14 days after ICH with H&E staining. As shown in Fig. 8A, B, the brain lesion volume in the GFP-ICH group and Nrn-ICH group was 5.69 ± 0.97 mm^3 and 2.70 ± 0.48 mm^3, respectively. Overexpression of Nrn significantly reduced ICH-induced brain lesions by 52.55% 14 days after ICH. No significant difference was observed in the water content of striatal, cortical and cerebellar regions 14 days after ICH among the GFP-Sham, GFP-ICH and Nrn-ICH groups (Fig. 8C).

To determine whether the PERK/ATF4 and Akt/mTOR signal pathways were involved in the Nrn-mediated brain recovery in the later stages of ICH, the levels of p-PERK, ATF4, p-Akt and p-mTOR in ipsilateral striatal tissue 14 days after ICH was detected by immunoblotting. The western blot results showed that p-PERK levels in the GFP-Sham, GFP-ICH and Nrn-ICH groups were not significantly different (Fig. 8D, F). However, ATF4 levels in the GFP-ICH group significantly increased by 455.13% ± 101.66% compared with those in the GFP-Sham group, whereas those in the Nrn-ICH group increased by 104.26% ± 40.98% compared with the GFP-Sham group, representing a 77.09% decrease compared with the GFP-ICH group (Fig. 8D, G). Compared with the GFP-Sham group, the level of p-Akt in the ipsilateral striatum of mice in the GFP-ICH group was significantly increased by 38.47% ± 16.27% (Fig. 8E, H). Similarly, the p-mTOR level in the ipsilateral striatum of mice in the GFP-ICH group was increased by 29.78% ± 9.10% (Fig. 8E, I). However, the p-Akt and p-mTOR levels in the ipsilateral striatum of mice in the Nrn-ICH group were at levels similar to those found in the GFP-Sham group (compared with the GFP-Sham group, the levels of p-Akt and p-mTOR in the Nrn-ICH group were decreased by 15.10% ± 7.89% and 9.89% ± 4.27%, respectively.) (Fig. 8E, H, I). The above results indicate that the PERK/ATF4 and Akt/mTOR pathways are involved in the protective effects of Nrn against neuronal death in the later stages after ICH.

To evaluate whether PERK and Akt signaling are the main pathways associated with the protective effect of Nrn, the intra-cerebroventricular infusion of GSK2656157 (a PERK signaling pathway inhibitor) and PI103 (a Akt signaling pathway inhibitor) were carried out, respectively.

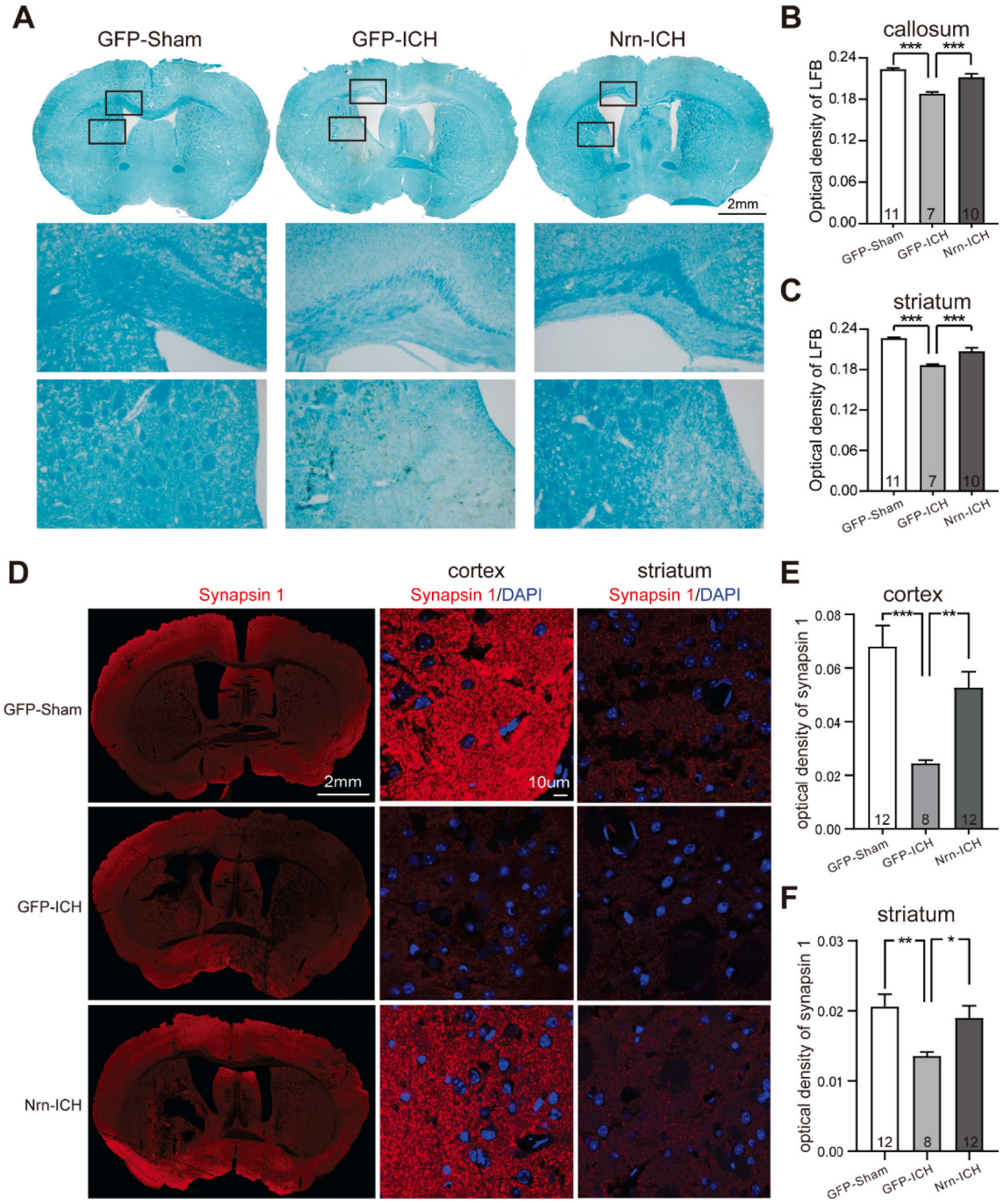

Fig. 7. Nrn preserved white matter integrity and synapse integrity.
A, Representative LFB staining in the GFP-Sham, GFP-ICH and Nrn-ICH group was performed 3 days after ICH. Middle, A high-magnification image of the corpus callosum from the boxed area in the above image; below, A high-magnification image of the striatum from the boxed area in the above image. B—C, Statistical histogram of the optical density of LFB staining in the corpus callosum and striatum (***$P < 0.001$ between groups connected by a straight line; one-way ANOVA). D, Representative synapsin 1 immunofluorescence in the GFP-Sham, GFP-ICH and Nrn-ICH group was performed 3 days after ICH. Middle, A high-magnification image of the cortex from the left image; Right, A high-magnification image of the striatum from the left image. E–F, Statistical histogram of the optical density of synapsin 1 staining in the cortex and striatum (*$P < 0.05$, **$P < 0.01$, ***$P < 0.001$ between groups connected by a straight line; one-way ANOVA).

As shown in Fig. 9A–E, both inhibitors effectively inhibited the expression of p-PERK, ATF4 and p-Akt. At the same time, the weight of the mice and results from the behavioral tests shown in Fig. 9F–H showed that the neuroprotective effect of Nrn was effectively blocked under the action of PERK and Akt signaling pathway inhibitors, indicating that Nrn overexpression plays a neuroprotective role by regulating the PERK and Akt signaling pathways.

4. Discussion

The neuroprotective effect of Nrn has recently been implicated in the pathophysiology of ischemic stroke (Zhao et al., 2017a) and in experimental subarachnoid hemorrhage (Zhang et al., 2017). In the present study, we investigated the effects of AAV-mediated overexpression of Nrn on hemorrhagic brain injury induced by ICH. We found that Nrn improved ICH-induced mouse sensory and motor behavioral deficits by

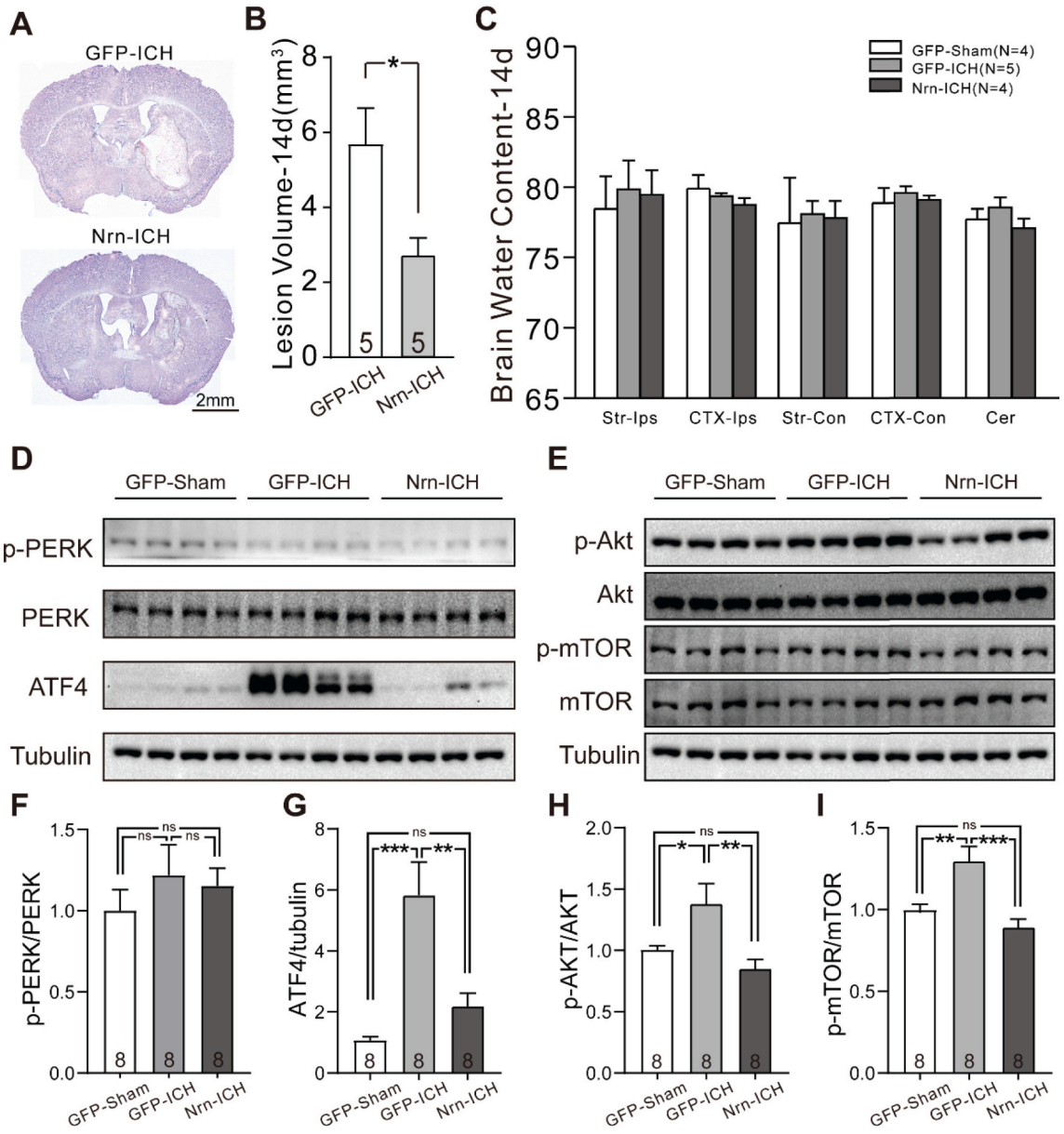

Fig. 8. Nrn reduced brain lesions and regulated the PERK/ATF4 and Akt/mTOR pathways 14 days after ICH.
A, Schematic diagram of H&E staining in the GFP-ICH and Nrn-ICH groups 14 days after ICH. B, Statistical histogram of the brain lesion volume ($*P < 0.05$ between groups connected by a straight line; two-sample t-test). C, Statistical histogram of water content in different brain areas 14 days after ICH, respectively. Str, striatum; CTX, Cortex; Cer, cerebellum; Ips: ipsilateral; Con, contralateral (one-way ANOVA). D, Representative western blot of PERK and ATF4 expression in the ipsilateral striatum of mice in the GFP-ICH and Nrn-ICH groups. E, Representative western blot of Akt and mTOR in the ipsilateral striatum of mice in the GFP-ICH and Nrn-ICH groups. F–G, Statistical histogram of PERK protein phosphorylation levels and ATF4 protein expression levels. H—I, Statistical histogram of Akt and mTOR protein phosphorylation levels (ns $P > 0.05$, $*P < 0.05$, $**P < 0.01$, $***P < 0.001$ between groups connected by a straight line; one-way ANOVA).

reducing brain lesions and edema and by inhibiting neuronal death and white matter and synapse integrity dysfunction. The effects of Nrn on reducing PERK/ATF4 levels and rescuing Akt/mTOR expression might be factors associated with the neuroprotective mechanisms of Nrn. Moreover, we showed for the first time that Nrn reversed ICH-induced dysfunctional electrophysiological activities in layer II/III pyramidal neurons of the motor cortex, which are receive signals from the affected striatum. Our study provides a new functional index of Nrn for the future study of ICH.

Nrn is a critical protein for dendritic outgrowth, maturation and axonal regeneration (Cantallops et al., 2000; Gao et al., 2016; Naeve et al., 1997a; Sato et al., 2012). It can be released into the extracellular space in a soluble-secreted form *in vivo*, and several studies have indicated that this soluble form has neurotrophic effects on mammalian neurons (Fujino et al., 2008; Naeve et al., 1997a). Nrn has a molecular weight of 11 kDa, and therefore, does not readily pass through the blood-brain barrier. We therefore performed overexpression studies by stereotaxically injecting AAV-Nrn virus into the striatum of mice, which was previously performed *via* hippocampal injection in a previous study (Zhao et al., 2015a). We found that Nrn protein levels in the ipsilateral striatum were significantly increased after injection of AAV-Nrn. Moreover, Nrn protein levels in the cortex, located above the striatum, were also increased. The increase in Nrn levels in the cortex were likely due to the spread of the AAV virus after infection, and/or secretion of Nrn, which may be associated with the Nrn-induced neurological outcome after ICH. a.

Secondary damage induced by ICH may occur through many parallel pathological pathways, such as oxidative stress, inflammation,

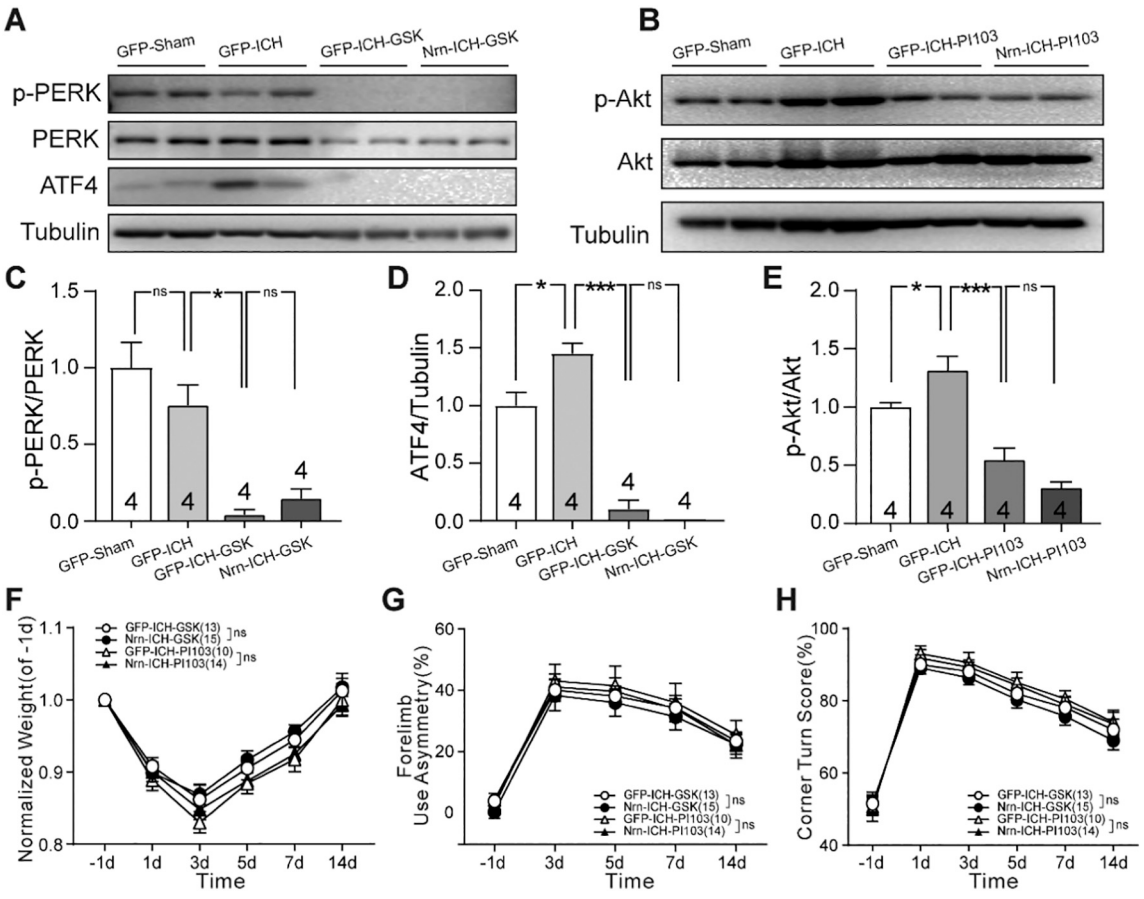

Fig. 9. PERK/ATF4 and Akt/mTOR signaling pathways are essential for Nrn-mediated protection.
A, Representative western blot of PERK and ATF4 expression in the ipsilateral striatum of mice in the distinct treatment groups 14 days after ICH. B, Representative western blot of Akt from the ipsilateral striatum in the GFP-ICH and Nrn-ICH groups. C–E, Statistical histogram of p-PERK, ATF4 and p-Akt protein expression levels (ns $P > 0.05$, $^{*}P < 0.05$, $^{**}P < 0.01$, $^{***}P < 0.001$ between groups connected by a straight line; one-way ANOVA). F—H, The relative weight curve, asymmetric forelimb used in the cylinder test and corner turn score in the corner test of each group at different time points (ns $P > 0.05$, two-way ANOVA).

cytotoxicity of blood, hypermetabolism and excitotoxicity (Ardizzone et al., 2004; Qureshi et al., 2003; Wagner et al., 2003; Xi et al., 2006). This pathogenesis ultimately leads to deadly brain edema with massive brain cell death (Xi et al., 2006). In this study, we found Nrn-ICH group have significantly smaller lesion volumes and trends toward alike hematoma volumes compared with GFP-ICH group, which is similar to many studies(Alim et al., 2019; Leclerc et al., 2018; Saand et al., 2019). Meanwhile, our data demonstrated that Nrn significantly reduced ICH-induced neuronal death, Consistent with previous studies on experimental subarachnoid hemorrhage(Zhang et al., 2017). These results suggest that neuritin has a neuronal protective function but does not contribute to hematoma clearance. However, although Nrn significantly decreased ICH induced cerebral edema 3 days after ICH, there was no significant effect on cerebral edema 14 days after ICH. This may be due to intrinsic recovery of neurons in the affected area at this later experimental stage in our experimental model. Both clinical cases and experimental studies show that early prevention of secondary injury after a primary insult to the brain is particularly important (Aronowski and Zhao, 2011). Our results also suggest that the neuroprotective effects of Nrn occurred at early stages after ICH, which likely enhanced functional recovery.

Increasing evidence has shown that after ICH, protein misfolding and accumulation in the endoplasmic reticulum (ER) lumen initiate ER stress and lead to mitochondrial apoptosis (Duan et al., 2017; Huang et al., 2018). The PERK/ATF4 pathway is considered a critical molecular pathway related to ER stress (Walter et al., 2015) and is implicated in cell death induced by early brain injury after subarachnoid hemorrhage and traumatic brain injury (Rubovitch et al., 2015; Yan et al., 2017). Consistent with previous studies, both the phosphorylation of PERK and its downstream effector ATF4 in striatal tissue from the GFP-ICH group 3 or 14 days after ICH were significantly increased. Our results indicated that Nrn effectively inhibited the ICH-induced high expression of PERK and ATF4, and that the PERK signaling pathway inhibitor GSK2656157 blocked the neuroprotective effects of Nrn. These results suggest that Nrn protects against ICH-induced neuronal injury and cell death by inhibiting the PERK/ATF4 pathway. Our previous study on cultured neurons and brain slices indicated that Nrn improved ion channel protein expression and enhanced synaptic transmission by activation of the insulin receptor (Lu et al., 2017; Yao et al., 2016). It may be worthwhile in future studies to determine if the effects of Nrn on the PERK/ATF4 pathway are mediated indirectly by the IR pathway or *via* another signaling pathway.

Akt is a serine/threonine kinase and has a critical role in promoting neuronal survival (Jo et al., 2012; Zhao et al., 2014). When Akt is activated, it phosphorylates a diverse number of protein substrates, including mTOR (Selvaraj et al., 2012; Terenzio et al., 2018). Our previous study indicated that Nrn activated the Akt/mTOR signaling pathway(Yao et al., 2012). In this study, phosphorylation of Akt/mTOR in the striatum of mice subject to ICH was significantly lower than controls at the acute phase. Specifically, Nrn reversed ICH-induced reductions in the phosphorylation of Akt/mTOR to those of baseline levels and PI103 effectively blocked the neuroprotective effects of Nrn. Coincidentally, this observation was similar with Yan's report in which the ratio of p-Akt/Akt decreased significantly at 12 h after subarachnoid

hemorrhage and reached a minimum at 72 h; moreover, PERK inhibition by the inhibitor significantly increased p-Akt and Bcl-2 levels and decreased Bax and caspase-3 expression, all of which were blocked by the co-administration of the selective Akt inhibitor (Yan et al., 2017). It is highly likely that Nrn suppresses PERK activity and enhances the subsequent Akt-related neuronal survival after ICH.

Our previous study demonstrated that virus-mediated overexpression of Nrn in the hippocampus increased the density of dendritic spines and reversed deficits in novel object associative recognition memory in mice, caused by exposure to extremely low-frequency (50 Hz) electromagnetic fields (Zhao et al., 2015a). In the current study, the effect of Nrn on synaptic plasticity and neuronal excitability was observed in layer II/III pyramidal neurons of the motor cortex in culture slices, which received signal projections from the striatum *in vivo*. sEPSCs, which regulate synaptic plasticity and homeostasis (Chung and Kavalali, 2006; Lee et al., 2004), and the firing frequency of APs, which are an index of the neuronal excitability, were reduced in cortical neurons after ICH. Reduced sEPSCs and AP frequency was likely due to the loss of input stimuli from projection neurons of the striatum, which are affected by neuronal cell death and white matter and synapse integrity dysfunction. Nrn significantly rescued the ICH-induced deficits by increasing sEPSCs and the AP frequency, which was likely the result of a reduction in ICH-induced edema and neuronal death in the striatum. Indeed, an increase in cortical Nrn may have direct effects on sEPSCs and AP frequency, as like its role on other neurons (Lu et al., 2017). Whether Nrn has a significant role in the formation of new circuits after ICH, possibly by increasing the density of dendritic spines (Zhao et al., 2015a).

In conclusion, our data show at first that Nrn improves neurological deficits in mice after ICH by reducing brain lesions and edema and inhibiting neuronal death and white matter or synapse integrity dysfunction, and that increased neuronal connections might be involved. However, since ICH-induced neuronal damage and consequent dysfunction are complex and multifactorial, except for the effects that we have observed in this study, it is still an open question whether Nrn also has a role in reducing cytotoxicity, inhibiting inflammation and forming new synapses that compensate for lost structural circuits.

Funding

This work was supported by grants from the National Natural Science Foundation of China (NSFC 31370827) and China Postdoctoral Science Foundation (2018M641915).

Author contributions

The corresponding author is responsible for ensuring that the descriptions are accurate and agreed by all authors. Yanai Mei and Junmei Lu conceived the idea, initiated the project, designed experiments, analyzed data and wrote the manuscript. With help from Zhaoyang Li for blinding, Junmei Lu performed the mouse models and behavioral experiments, western blotting, tissue analyses and electrophysiological record. Qianru Zhao and Dongdong Liu performed biostatistical analysis.

Declaration of Competing Interest

The authors declare no competing financial interests.

References

Alim, I., et al., 2019. Selenium drives a transcriptional adaptive program to block ferroptosis and treat stroke. Cell. 177, 1262–1279 e25.
Ardizzone, T.D., et al., 2004. Glutamate receptor blockade attenuates glucose hypermetabolism in perihematomal brain after experimental intracerebral hemorrhage in rat. Stroke. 35, 2587–2591.
Aronowski, J., Zhao, X., 2011. Molecular pathophysiology of cerebral hemorrhage: secondary brain injury. Stroke. 42, 1781–1786.
Barratt, H.E., et al., 2014. Mouse intracerebral hemorrhage models produce different degrees of initial and delayed damage, axonal sprouting, and recovery. J. Cereb. Blood Flow Metab. 34, 1463–1471.
Cai, P., et al., 2015. Recombinant ADAMTS 13 attenuates brain injury after intracerebral hemorrhage. Stroke. 46, 2647–2653.
Cantallops, I., et al., 2000. Postsynaptic CPG15 promotes synaptic maturation and presynaptic axon arbor elaboration in vivo. Nat. Neurosci. 3, 1004–1011.
Cao, J., et al., 2018. Leucine-rich repeat kinase 2 aggravates secondary brain injury induced by intracerebral hemorrhage in rats by regulating the P38 MAPK/Drosha pathway. Neurobiol. Dis. 119, 53–64.
Chaudhary, N., et al., 2019. Hemorrhagic stroke-Pathomechanisms of injury and therapeutic options. CNS Neurosci Ther. 25, 1073–1074.
Chen, S., et al., 2014. Progressing haemorrhagic stroke: categories, causes, mechanisms and managements. J. Neurol. 261, 2061–2078.
Chung, C., Kavalali, E.T., 2006. Seeking a function for spontaneous neurotransmission. Nat. Neurosci. 9, 989–990.
Dai, S., et al., 2019. Minocycline attenuates brain injury and iron overload after intracerebral hemorrhage in aged female rats. Neurobiol. Dis. 126, 76–84.
Duan, X.-C., et al., 2017. Roles of autophagy and endoplasmic reticulum stress in intracerebral hemorrhage-induced secondary brain injury in rats. CNS Neurosci. Therap. 23, 554–566.
Fujino, T., et al., 2008. cpg15 and cpg15-2 constitute a family of activity-regulated ligands expressed differentially in the nervous system to promote neurite growth and neuronal survival. J. Comp. Neurol. 507, 1831–1845.
Gao, R., et al., 2016. Exogenous neuritin promotes nerve regeneration after acute spinal cord injury in rats. Hum. Gene Ther. 27, 544–554.
He, Y.L., et al., 2013. Expression of candidate plasticity-related gene 15 is increased following traumatic brain injury. Neurol. Res. 35, 174–180.
Huang, Q., et al., 2018. DiDang tang inhibits endoplasmic reticulum stress-mediated apoptosis induced by oxygen glucose deprivation and intracerebral hemorrhage through blockade of the GRP78-IRE1/PERK pathways. Front. Pharmacol. 9.
Jo, H., et al., 2012. Small molecule-induced cytosolic activation of protein kinase Akt rescues ischemia-elicited neuronal death. Proc. Natl. Acad. Sci. U. S. A. 109, 10581–10586.
Karuppagounder, S.S., et al., 2016. Therapeutic targeting of oxygen-sensing prolyl hydroxylases abrogates ATF4-dependent neuronal death and improves outcomes after brain hemorrhage in several rodent models. Sci. Transl. Med. 8, 328ra29.
Katsuki, H., Hijioka, M., 2017. Intracerebral hemorrhage as an axonal tract injury disorder with inflammatory reactions. Biol. Pharm. Bull. 40, 564–568.
Le Jan, S., et al., 2006. Characterization of the expression of the hypoxia-induced genes neuritin, TXNIP and IGFBP3 in cancer. FEBS Lett. 580, 3395–3400.
Leclerc, J.L., et al., 2018. Increased brain hemopexin levels improve outcomes after intracerebral hemorrhage. J. Cereb. Blood Flow Metab. 38, 1032–1046.
Lee, J.K., et al., 2004. Nogo receptor antagonism promotes stroke recovery by enhancing axonal plasticity. J. Neurosci. 24, 6209–6217.
Li, M., et al., 2016. Methazolamide improves neurological behavior by inhibition of neuron apoptosis in subarachnoid hemorrhage mice. Sci. Rep. 6, 35055.
Li, H., et al., 2018. Critical role for Annexin A7 in secondary brain injury mediated by its phosphorylation after experimental intracerebral hemorrhage in rats. Neurobiol. Dis. 110, 82–92.
Liu, Y., et al., 2018. Characterization of axon damage, neurological deficits, and histopathology in two experimental models of intracerebral hemorrhage. Front. Neurosci. 12, 928.
Lu, J., et al., 2011. Troxerutin protects against high cholesterol-induced cognitive deficits in mice. Brain. 134, 783–797.
Lu, J.M., et al., 2017. Neuritin enhances synaptic transmission in medial prefrontal cortex in mice by increasing CaV3.3 surface expression. Cereb. Cortex 27, 3842–3855.
Lule, S., et al., 2020. Cell-specific activation of RIPK1 and MLKL after intracerebral hemorrhage in mice. J. Cereb. Blood Flow Metab. https://doi.org/10.1177/0271678X20973609.
Murphy, T.H., Corbett, D., 2009. Plasticity during stroke recovery: from synapse to behaviour. Nat. Rev. Neurosci. 10, 861–872.
Naeve, G.S., et al., 1997a. Neuritin: a gene induced by neural activity and neurotrophins that promotes neuritogenesis. Proc. Natl. Acad. Sci. U. S. A. 94, 2648–2653.
Naeve, G.S., et al., 1997b. Neuritin: a gene induced by neural activity and neurotrophins that promotes neuritogenesis. Proc. Natl. Acad. Sci. U. S. A. 94, 2648–2653.
Nedivi, E., et al., 1993. Numerous candidate plasticity-related genes revealed by differential Cdna cloning. Nature. 363, 718–722.
Pu, H., et al., 2019. Protease-independent action of tissue plasminogen activator in brain plasticity and neurological recovery after ischemic stroke. Proc. Natl. Acad. Sci. U. S. A. 116, 9115–9124.
Qureshi, A.I., et al., 2003. Extracellular glutamate and other amino acids in experimental intracerebral hemorrhage: an in vivo microdialysis study. Crit. Care Med. 31, 1482–1489.
Rickhag, M., et al., 2007. Rapid and long-term induction of effector immediate early genes (BDNF, Neuritin and arc) in peri-infarct cortex and dentate gyrus after ischemic injury in rat brain. Brain Res. 1151, 203–210.
Rubovitch, V., et al., 2015. The neuroprotective effect of Salubrinal in a mouse model of traumatic brain injury. NeuroMolecular Med. 17, 58–70.
Rynkowski, M.A., et al., 2008. A mouse model of intracerebral hemorrhage using autologous blood infusion. Nat. Protoc. 3, 122–128.
Saand, A.R., et al., 2019. Systemic inflammation in hemorrhagic strokes - a novel neurological sign and therapeutic target? J. Cereb. Blood Flow Metab. 39, 959–988.

Sato, H., et al., 2012. Thalamus-derived molecules promote survival and dendritic growth of developing cortical neurons. J. Neurosci. 32, 15388–15402.
Schallert, T., et al., 2000. CNS plasticity and assessment of forelimb sensorimotor outcome in unilateral rat models of stroke, cortical ablation, parkinsonism and spinal cord injury. Neuropharmacology. 39, 777–787.
Selvaraj, S., et al., 2012. Neurotoxin-induced ER stress in mouse dopaminergic neurons involves downregulation of TRPC1 and inhibition of AKT/mTOR signaling. J. Clin. Invest. 122, 1354–1367.
Shen, F., et al., 2021. Rbfox-1 contributes to CaMKIIalpha expression and intracerebral hemorrhage-induced secondary brain injury via blocking micro-RNA-124. J. Cereb. Blood Flow Metab. 41, 530–545.
Son, H., et al., 2012. Neuritin produces antidepressant actions and blocks the neuronal and behavioral deficits caused by chronic stress. Proc. Natl. Acad. Sci. U. S. A. 109, 11378–11383.
Terenzio, M., et al., 2018. Locally translated mTOR controls axonal local translation in nerve injury. Science. 359, 1416–1421.
Wagner, K.R., et al., 2003. Heme and iron metabolism: role in cerebral hemorrhage. J. Cereb. Blood Flow Metab. 23, 629–652.
Walter, F., et al., 2015. Imaging of single cell responses to ER stress indicates that the relative dynamics of IRE1/XBP1 and PERK/ATF4 signalling rather than a switch between signalling branches determine cell survival. Cell Death Differ. 22, 1502–1516.
Wang, Z., et al., 2018. Treatment of secondary brain injury by perturbing postsynaptic density protein-95-NMDA receptor interaction after intracerebral hemorrhage in rats. J. Cereb. Blood Flow Metab. 39, 1588–1601.
Xi, G., et al., 2006. Mechanisms of brain injury after intracerebral haemorrhage. Lancet Neurol. 5, 53–63.
Xu, J., et al., 2020. IL-4/STAT6 signaling facilitates innate hematoma resolution and neurological recovery after hemorrhagic stroke in mice. Proc. Natl. Acad. Sci. U. S. A. 117, 32679–32690.
Yan, F., et al., 2017. Pharmacological inhibition of PERK attenuates early brain injury after subarachnoid hemorrhage in rats through the activation of Akt. Mol. Neurobiol. 54, 1808–1817.
Yang, J., et al., 2015. Prognostic significance of perihematomal edema in acute intracerebral hemorrhage pooled analysis from the intensive blood pressure reduction in acute cerebral hemorrhage trial studies. Stroke 46, 1009.
Yang, H., et al., 2020. HDAC inhibition reduces white matter injury after intracerebral hemorrhage. J. Cereb. Blood Flow Metab. 41, 958–974 .
Yao, J.J., et al., 2012. Neuritin activates insulin receptor pathway to up-regulate Kv4.2-mediated transient outward K+ current in rat cerebellar granule neurons. J. Biol. Chem. 287, 41534–41545.
Yao, J.J., et al., 2016. Neuritin up-regulates Kv4.2 alpha-subunit of potassium channel expression and affects neuronal excitability by regulating the calcium-calcineurin-NFATc4 signaling pathway. J. Biol. Chem. 291, 17369–17381.
Zhang, Y.H., et al., 2014. Cytotoxic genes from traditional Chinese medicine inhibit tumor growth both in vitro and in vivo. J. Integr. Med. 12, 483–494.
Zhang, H., et al., 2017. Neuritin attenuates early brain injury in rats after experimental subarachnoid hemorrhage. Int. J. Neurosci. 127, 1087–1095.
Zhao, T., et al., 2014. Pretreatment by evodiamine is neuroprotective in cerebral ischemia: up-regulated pAkt, pGSK3beta, down-regulated NF-kappaB expression, and ameliorated BBB permeability. Neurochem. Res. 39, 1612–1620.
Zhao, Q.R., et al., 2015a. Neuritin reverses deficits in murine novel object associative recognition memory caused by exposure to extremely low-frequency (50 Hz) electromagnetic fields. Sci. Rep. 5, 11768.
Zhao, X.R., et al., 2015b. Pleiotropic role of PPARgamma in intracerebral hemorrhage: an intricate system involving Nrf2, RXR, and NF-kappaB. CNS Neurosci. Ther. 21, 357–366.
Zhao, J.J., et al., 2017a. Soluble cpg15 from astrocytes ameliorates neurite outgrowth recovery of hippocampal neurons after mouse cerebral ischemia. J. Neurosci. 37, 1628–1647.
Zhao, Q., et al., 2017b. Thioredoxin-interacting protein links endoplasmic reticulum stress to inflammatory brain injury and apoptosis after subarachnoid haemorrhage. J. Neuroinflammation 14, 104.
Zhao, H., et al., 2018a. P2X7 receptor-associated programmed cell death in the pathophysiology of hemorrhagic stroke. Curr. Neuropharmacol. 16, 1282–1295.
Zhao, Q.R., et al., 2018b. Neuritin promotes neurite and spine growth in rat cerebellar granule cells via L-type calcium channel-mediated calcium influx. J. Neurochem. 147, 40–57.